FRP-Reinforced Wood as Structural Material

By Nikolaos Plevris[1] and Thanasis C. Triantafillou,[2]
Associate Member, ASCE

ABSTRACT: Advanced forms of wood construction can enable contemporary wood structures such as bridges to be competitive with those constructed from any other conventional material. This paper presents the results of an analytical and experimental investigation of a new form of wood construction involving external bonding of thin fiber-reinforced plastic (FRP) sheets on the tension zones of wood beams and beam columns using epoxy resins. Here, we examine the effect of external composite reinforcement on the collapse mechanisms and loads, the stiffness and the curvature ductility of hybrid FRP wood members under a combination of bending moments and axial forces. We then give the results of three-point bending and eccentric compression tests confirming our analysis. The analysis is extended to establish a methodology for the optimum selection of the FRP reinforcement to optimize mechanical performance.

INTRODUCTION

Wood is a unique construction material. It stands alone in many characteristics when compared with man-made structural materials such as concrete, steel, brick, and reinforced plastics. Although wood structures have played an important role in construction, they have acquired a reputation for impermanence and limited application. Improved design, preservative treating methods, and advanced forms of wood member construction (reinforced wood) can enable contemporary wood structures such as bridges to be as permanent and economically competitive as those constructed from any other conventional material.

Wood members have been reinforced using many techniques. Steel bars have been used as glulam reinforcement (e.g., Lantos 1970; Dziuba 1985; Bulleit et al. 1989). Steel and aluminum plates have been placed between laminations both vertically and horizontally (Sliker 1962; Borgin et al. 1968; Stern and Kumar 1973; Coleman and Hurst 1974; Hoyle 1975). One unique attempt has been made to prestress glulam using stressed steel plates bonded on the tension face with epoxy adhesives (Peterson 1965). Fiberglass has been used in the faces of wood-core sandwich panels (Biblis 1965) and as external reinforcement of plywood ("Basic" 1972; Mitzner 1973). High-strength steel wire embedded in an epoxy matrix has been used to replace tension laminations of wood beams (Krueger 1973; Krueger and Eddy 1974; Krueger and Sandberg 1974; Kobetz and Krueger 1976). Finally, glulam has been prestressed using stranded cable (Bohannan 1962). Nevertheless, none of these reinforcement techniques has reached full commercialization; most of them appear very time-consuming, requiring complicated steps, and others are characterized by lack of reliability as far as long-term performance is concerned (especially the methods involving external bonding of metal

[1]Grad. Res. Asst., Dept. of Civ. Engrg., Massachusetts Inst. of Tech., Cambridge, MA 02139.

[2]Asst. Prof. of Civ. Engrg., Dept. of Civ. Engrg., Massachusetts Inst. of Tech., Cambridge, MA.

plates), while the methods using nonmetallic reinforcement lack systematic analysis procedures.

A new form of wood construction is analyzed in this study, involving reinforcing wood members with advanced fiber-reinforced plastic (FRP) composite materials. The method involves external bonding of thin FRP sheets on the tension zones of wood structures using epoxy resins and yields members with enhanced strength, stiffness, and ductility characteristics. The composite sheets are made of unidirectional, continuous fibers (e.g., carbon) bonded together with a matrix such as epoxy resin, resulting in a lightweight and high-mechanical-performance system. A wood beam reinforced with a thin carbon FRP (CFRP) sheet is shown in Fig. 1.

The technique of reinforcing structures with externally epoxy-bonded FRP laminates on the tension zones is not new. Research work by Meier (1987), Kaiser (1989), Iyer et al. (1989), Saadatmanesh and Ehsani (1989, 1990), Ritchie et al. (1990), and Triantafillou and Plevris (1991), has established the flexural behavior of reinforced concrete beams strengthened with external FRP reinforcement. These studies have demonstrated that unidirectional composite sheets are ideal in playing the role of tension reinforcement as well as in providing a means of increasing the stiffness char-
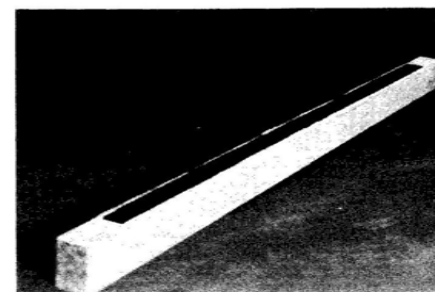

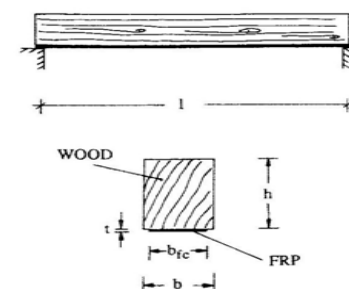FIG. 1. Photograph of FRP-Reinforced Wood Beam

FIG. 2. Wood Beam of Span *l* Reinforced with FRP Sheet and Cross-Sectional Properties

acteristics of a structure. The technique has been extended by prestressing the laminates before bonding them on the beams (Triantafillou and Deskovic 1991).

In this paper, we focus on developing a fundamental understanding of the behavior of the FRP-reinforced wood system. We examine the effect of externally bonded composite materials on the failure mechanisms, the stiffness, and the ductility of the hydrid member subject to a combination of bending and axial loads, and give the results of three-point bending and eccentric compression tests confirming our analysis. An analytical solution is then used in establishing a methodology for the optimum design of the hybrid FRP wood system to maximize mechanical performance.

ANALYSIS

A typical hybrid FRP wood member of span l is shown in Fig. 2. The wood section has a depth h and a width b, and the fiber-composite sheet has a thickness t and a width b_{fc}. The FRP material is idealized as linear elastic with Young's modulus E_{fc} and tensile failure strain ε_{fc}^*. The assumed uniaxial stress-strain relationship for wood is that proposed by Bazan (1980) and modified by Buchanan (1990). Tension behavior is assumed to be linear elastic with failure occurring at a stress f_t, corresponding to strain ε_t. In compression, failure occurs at a stress f_c, corresponding to strain ε_c; for strains higher than ε_c, the stress-strain relationship is described by a falling
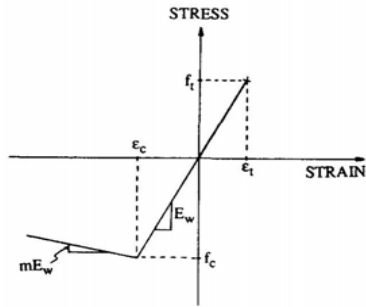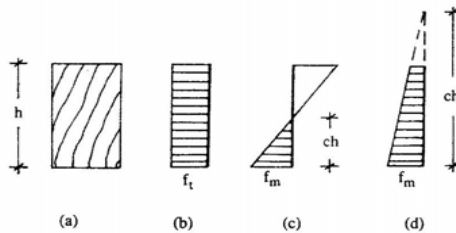

FIG. 3. Stress-Strain Relationship for Wood

FIG. 4. Tension Stress Diagrams in Wood Cross Section
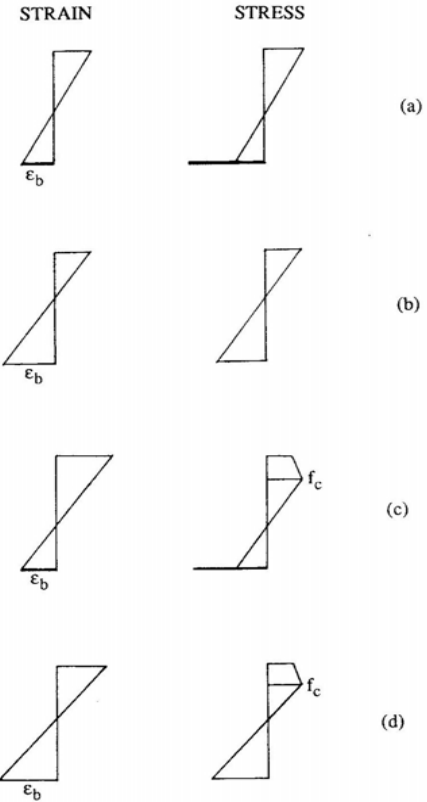
302

FIG. 5. Strain Profiles and Stress Diagrams Corresponding to Following States: (a) Both Wood and FRP are Linear-Elastic; (b) Wood is Linear-Elastic, FRP has Ruptured; (c) Wood has Yielded and FRP is Linear-Elastic; and (d) Wood has Yielded and FRP has Ruptured

branch, the slope of which is a constant ratio, m, of the Young's modulus, E_w (Fig. 3).

Bending Strength

One major problem encountered when developing flexural strength models for wood is the stress distribution effect, which accounts for the extreme fiber tensile stress at failure f_m being greater in bending than in axial tension. Buchanan (1986) has quantified the stress distribution effect using Weibull's (1939) brittle fracture theory. For the section shown in Fig. 4(a), the tensile strength shown in Fig. 4(b) is related to the extreme fiber tensile stress at failure in Figs. 4(c) and 4(d) using

303
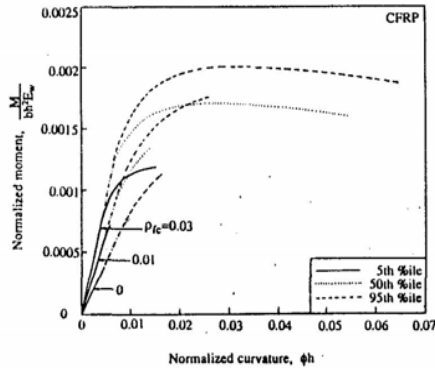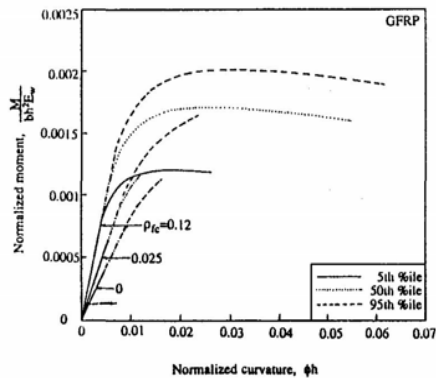
FIG. 6. Moment-Curvature Relationships for Various FRP Area Fractions and Wood Strengths: (a) CFRP; and (b) GFRP

$$f_m = \left(\frac{c}{1+k}\right)^{-1/k} f_t \quad \dots\dots\dots\dots\dots\dots\dots\dots\dots\dots\dots\dots\dots \quad (1)$$

if the neutral axis is inside the section, or

$$f_m = \left\{\frac{c}{1+k}\left[1 - \left(1 - \frac{1}{c}\right)^{k+1}\right]\right\}^{-1/k} f_t \quad \dots\dots\dots\dots\dots\dots \quad (2)$$

if the neutral axis is outside the section. The stress distribution parameter k reflects the variability in strength properties within the depth of a member, and c is the depth of the neutral axis from the tensile face as a ratio of the depth h of the cross section. For this work, it has not been necessary to consider any other size effects, because the objective is to predict bending strength of FRP-reinforced wood from tensile and compressive strengths of members of the same cross-sectional dimensions.

TABLE 1. Material Properties Used in Analysis

| Material (1) | E_w (GPa) (2) | m (3) | 50th Percentile[a] | | 5th Percentile[a] | | 95th Percentile[a] | | k (10) | E_{fc} (GPa) (11) | ε_{fc}^* (12) |
			f_c (MPa) (4)	f_t (MPa) (5)	f_c (MPa) (6)	f_t (MPa) (7)	f_c (MPa) (8)	f_t (MPa) (9)			
Wood	8.3	0.02	32.0	29.0	22.5	14.0	37.5	46.5	10.0	—	—
CFRP	—	—	—	—	—	—	—	—	—	186	0.0075
GFRP	—	—	—	—	—	—	—	—	—	51	0.0250

[a]pth percentile corresponds to the value of the strength x such that $p\%$ of the measurements have values less than x, while $(100 - p)\%$ have values greater than x.

The flexural behavior of FRP-reinforced wood beams is fully described when the moment-curvature (M-ϕ) relationship is established for the cross section. A closed-form solution for the M-ϕ curve is impossible to obtain due to the material nonlinearity involved, in particular, the stress distribution effect. In this study, the problem was approached numerically: A computer program was written that, given the fiber-composite material area fraction ρ_{fc} (being defined as the ratio $b_{fc}t/bh$, see Fig. 2), increments the strain at the wood bottom fiber, ε_b, until either the wood fractures (when $\varepsilon_b = f_m/E_w$) or no solution is possible, because force equilibrium at the cross section is violated. In the last case, ε_b has to decrease again and so does the moment M, but the curvature ϕ increases, resulting in a plastic hinge behavior. During this incremental procedure the depth of the neutral axis changes, making the continuous updating of the wood strength, f_m, a necessity [see (1) and (2)].

At failure of the system, i.e., when the extreme fiber tensile stress in wood equals f_m, the compressive zone may have yielded or not, while the composite sheet may have ruptured or not. Rupture of the FRP preceeds failure of the member when the ultimate strain of the fiber composite ε_{fc}^* is smaller than f_m/E_w; and compressive yield occurs when the tensile strength of wood and/or the area fraction ρ_{fc} of the composite sheet are relatively high.

Each value of the extreme tensile fiber strain ε_b is associated with one of the following states: Both wood and FRP are linear-elastic; wood is linear-elastic and FRP has ruptured; wood has yielded and FRP is linear-elastic; and wood has yielded and FRP has ruptured. The strain profiles and stress diagrams corresponding to each of these states are shown in Fig. 5. From the geometry of the stress diagrams and by taking equilibrium of forces, it is possible to define the location of the neutral axis. The bending moment M is then calculated by taking moments of the internal forces about the neutral axis. The equations describing the interaction between the bending moment M and the axial force P corresponding to the states described earlier are summarized next.

- Both wood and FRP linear-elastic:

$$\frac{M}{bh^2E_w} = \frac{C(c+2) - Tc}{3} + \frac{1}{2\left(\rho_{fc}\dfrac{E_{fc}}{E_W} + 1\right)}\frac{P}{bhE_w} \quad \dots\dots\dots \quad (3)$$
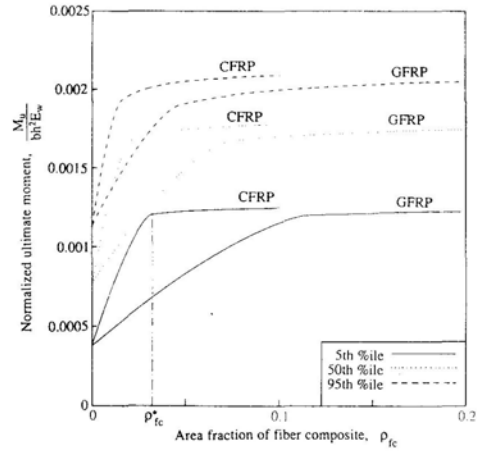
FIG. 7. Dependence of Ultimate Bending Capacity on CFRP and GFRP Area Fraction for Various Wood Strengths
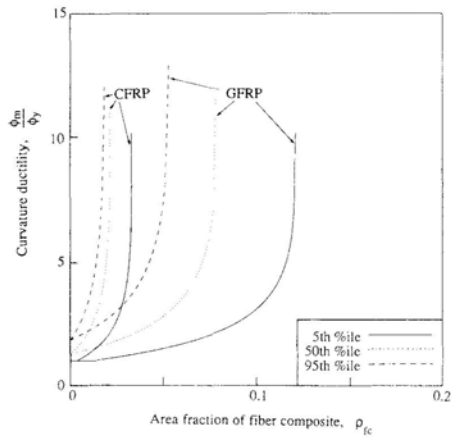

FIG. 8. Curvature Ductility Ratio as Function of CFRP and GFRP Area Fraction for Various Wood Strengths

where

$$T = \frac{c}{2}\,\varepsilon_b \quad \dotfill \quad (4a)$$

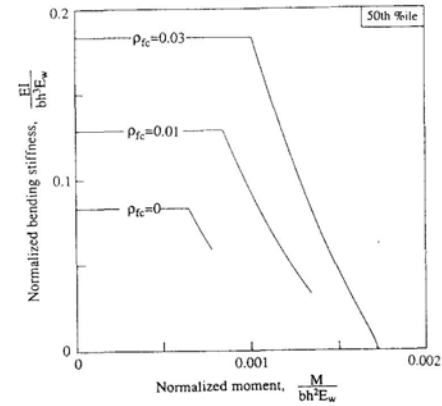$$C = \frac{(1 - c)^2}{2c}\,\varepsilon_b \quad \dotfill \quad (4b)$$

306

FIG. 9. Effect of Fiber-Composite Area Fraction on Bending Stiffness of CFRP-Reinforced Wood

$$c = \frac{1}{2\left(\rho_{fc}\dfrac{E_{fc}}{E_w} + 1 - \dfrac{P}{bhE_w}\dfrac{1}{\varepsilon_b}\right)} \quad \dotfill \quad (4c)$$

under the conditions $\varepsilon_b \le \varepsilon_{fc}^*$, $(1 - c)\varepsilon_b/c \le \varepsilon_c$, and $\varepsilon_b \le f_m/E_w$.
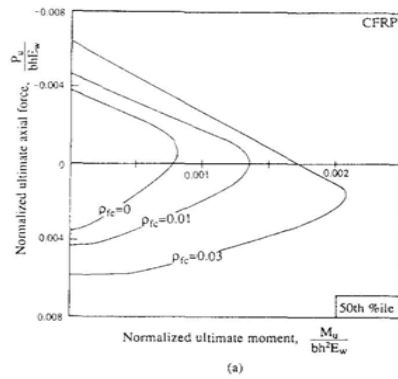
- Wood linear elastic and FRP ruptured:
  This is the same as in previous state but with $\rho_{fc} = 0$, under the conditions $\varepsilon_b \ge \varepsilon_{fc}^*$, $(1 - c)\varepsilon_b/c \le \varepsilon_c$ and $\varepsilon_b \le f_m/E_w$.

- Wood yield and FRP linear-elastic:

$$\frac{M}{bh^2E_w} = C_2\left\{1 - \left[1 - \left(\frac{\varepsilon_c}{\varepsilon_b} + 1\right)c\right]\frac{\left[\dfrac{(3 + m)}{m}\dfrac{c}{(c - 1)}\dfrac{\varepsilon_c}{\varepsilon_b} + 1\right]}{\left[\dfrac{(2 + m)}{m}\dfrac{c}{(c - 1)}\dfrac{\varepsilon_c}{\varepsilon_b} + 1\right]}\right\}$$

$$+ C_1c\left(1 + \frac{2}{3}\frac{\varepsilon_c}{\varepsilon_b}\right) - \frac{Tc}{3} + \frac{1}{2\left(\rho_{fc}\dfrac{E_{fc}}{E_w} + 1\right)}\frac{P}{bhE_w} \quad \dotfill \quad (5)$$
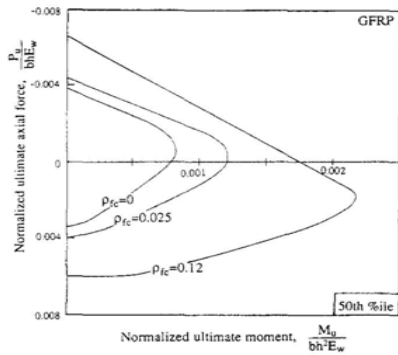
where

$$T = \frac{c}{2}\,\varepsilon_b \quad \dotfill \quad (6a)$$

$$C_1 = \frac{c}{2}\frac{\varepsilon_c^2}{\varepsilon_b} \quad \dotfill \quad (6b)$$

307

FIG. 10. Effect of Fiber-Composite Area Fraction on Bending Moment-Axial Force Interaction Diagram for FRP-Reinforced Wood: (a) CFRP; and (b) GFRP
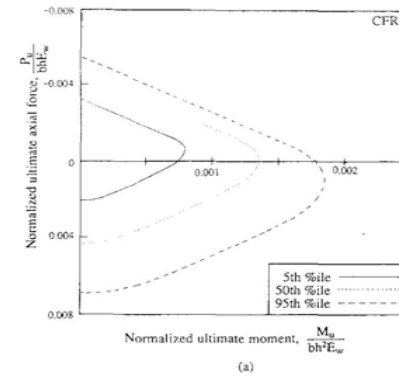
$$C_2 = \frac{1}{2}\left[1 - c\left(\frac{\varepsilon_c}{\varepsilon_b} + 1\right)\right]\left[(2 + m)\varepsilon_c + m\left(1 - \frac{1}{c}\right)\varepsilon_b\right] \quad \dots (6c)$$

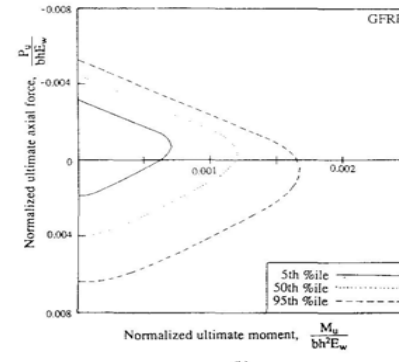and c is given by solving the following equation:

$$(1 + m)\left(1 + \frac{\varepsilon_c}{\varepsilon_b}\right)^2 c^2$$

$$+ \left[2\rho_{fc}\frac{E_{fc}}{E_w} - 2(1 + m)\frac{\varepsilon_c}{\varepsilon_b} - 2m - \frac{2}{\varepsilon_b}\frac{P}{bhE_w}\right]c + m = 0 \quad \dots (7)$$

under the conditions $\varepsilon_b \leq \varepsilon_{fc}^*$, $(1 - c)\varepsilon_b/c \geq \varepsilon_c$, $\varepsilon_c(1 + m) + m\varepsilon_b(c - 1)/c \geq 0$ and $\varepsilon_b \leq f_m/E_w$.

- Wood yield and FRP ruptured:

FIG. 11. Effect of Wood Strength Bending Moment-Axial Force Interaction Diagram for FRP-Reinforced Wood: (a) CFRP, $\rho_{fc} = 0.01$; and (b) GFRP, $\rho_{fc} = 0.025$

This is the same as in the previous state but with $\rho_{fc} = 0$, under the conditions $\varepsilon_b \geq \varepsilon_{fc}^*$, $(1 - c)\varepsilon_b/c \geq \varepsilon_c$, $\varepsilon_c(1 + m) + m\varepsilon_b(c - 1)/c \geq 0$ and $\varepsilon_b \geq f_m/E_w$.

To obtain the pure bending strength without axial force, P must be set equal to zero and the maximum moment must be obtained from the moment-curvature curve.

The role of wood strength and composite material area fraction in establishing the moment-curvature curve is illustrated in Figs. 6(a), and 6(b) for carbon FRP and glass FRP-reinforced wood, respectively. It is remarkable that by increasing the area of the external reinforcement, a transition from brittle collapse (linear M-ϕ relationship) to ductile failure (nonlinear M-ϕ curve) is possible. Furthermore, the bending moment of high-strength wood with rather heavy FRP reinforcement reaches a peak and begins to decrease, as shown in Fig. 6, but tension stresses continue to increase until
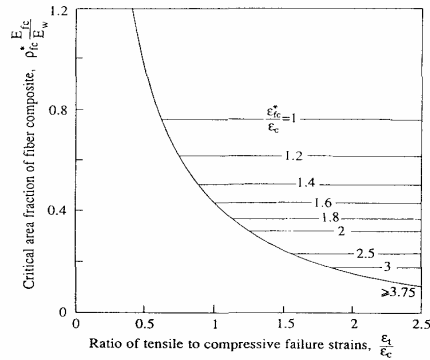
FIG. 12. Critical Area Fraction of Fiber Composite as Function of Material Properties for $k = 10$ and $m = 0.02$

TABLE 2. CFRP Area Fraction of Beams Tested (Series B)

Number of beams (1)	CFRP thickness (t) (mm) (2)	CFRP area fraction (ρ_{fc}) (3)
5	—	0
3	0.20	0.0033
5	0.41	0.0067
3	0.86	0.0143
3	2.44	0.0403

TABLE 3. Description of Uniaxial Stress-Strain Relationship for Wood Used in Experimental Procedure

Specimen series (1)	Young's modulus E_w, average value (GPa) (2)	Coefficient of variation (3)	Compressive strength f_c, average value (MPa) (4)	Coefficient of variation (5)	Tensile strength f_t, average value (MPa) (6)	Coefficient of variation (7)	m, average value (8)	Coefficient of variation (9)
B	12.28	0.027	63.86	0.056	100.94	0.13	0.04	0.06
BC	12.30	0.030	76.26	0.060	89.79	0.15	0.09	0.05

rupture occurs in the tension zone at a moment below the peak value. Fig. 6 and all subsequent figures in this section are based on the material properties listed in Table 1, which are typical of fir lumber, CFRP, and GFRP (Hull 1981; Bodig and Jayne 1982).

The important effect of the FRP area fraction on the ultimate moment is shown in Fig. 7 for two different composites. The bending strength increases almost linearly with ρ_{fc} up to a critical value, beyond which it becomes almost constant, independent of the type of composite material used.
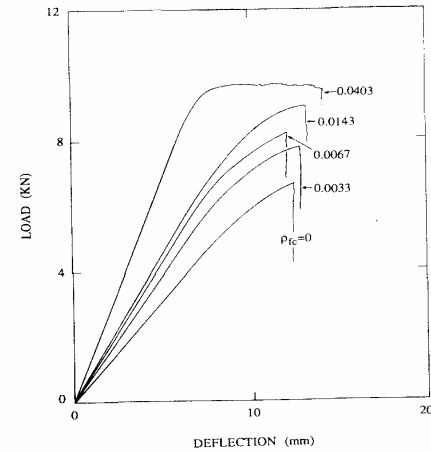
DEFLECTION (mm)

FIG. 13. Load-Deflection Curves for CFRP-Reinforced Wood Beams in Three-Point Bending

Ductility and Stiffness

The relationship between curvature ductility and FRP area fraction for two types of composite materials and a range of wood strengths is shown in Fig. 8. Ductility here is defined as the ratio of the maximum curvature ϕ_m to the curvature at first yield in the compression zone, ϕ_y. This relationship is described by an almost exponentially increasing branch, reflecting a very beneficial effect of the FRP on the ductility of the system.

Using the incremental equation $EI = \Delta M/\Delta \phi$ and the moment-curvature relationships obtained earlier, the flexural rigidity EI can be established as a function of the bending moment M. The effect of FRP area fraction on the rigidity of the member is shown in Fig. 9 for CFRP-reinforced wood; even a small ρ_{fc} (1%) can result in a stiffness increase on the order of 60% initially, and even higher when wood compressive yield occurs.

Bending Moment-Axial Force Interaction

The computer model based on the analysis in this paper was used to obtain bending moment-axial force interaction diagrams for typical wood materials reinforced with thin CFRP or GFRP sheets. Fig. 10 illustrates how the interaction diagrams evolve for various FRP area fractions, and Fig. 11 gives the interaction diagrams corresponding to one particular FRP area fraction and various wood strengths. A number of interesting observations can be made. A small increase in ρ_{fc} results in significant improvement of both the bending moment and the axial force capacity. For relatively high values of ρ_{fc}, the nose of the interaction curve is near or below the horizontal axis, producing a linear interaction between axial compression and bending. Furthermore, for a given FRP area fraction, the nose of the curve moves lower as the wood strength increases. This has also been found to be true when $\rho_{fc} = 0$ (Buchanan 1986).

TABLE 4. Measured and Calculated Failure Loads for FRP Wood Beams (Series B)

| ρ_{fc} (1)	Average measured failure load (kN) (2)	Calculated failure load (kN) (3)
0	6.74	6.95
0.0033	7.50	7.55
0.0067	8.58	8.56
0.0143	9.44	10.34
0.0403	10.72	11.99

Fiber Composite Material Selection

From the analysis presented previously, it is clear that there is a critical value of the external reinforcement area fraction, ρ_{fc}^*, beyond which the member's bending moment capacity levels off (see Fig. 7). It can be shown that ρ_{fc}^* corresponds to the transition from a wood rupture mechanism to plastic hinge behavior. Furthermore, the critical FRP area fraction depends on three parameters only: the ratio of the tensile to the compressive failure strain of wood, $\varepsilon_t/\varepsilon_c$, the ratio of the FRP ultimate strain to the wood compressive yield strain, $\varepsilon_{fc}^*/\varepsilon_c$, and the ratio of the elastic modulus of FRP to the elastic modulus of wood, E_{fc}/E_w. The critical FRP area fraction is given in the diagram of Fig. 12 (corresponding to $k = 10$ and $m = 0.02$) for a wide range of material properties. Using the critical ρ_{fc} may not be a cost-effective solution. Fortunately, significant increases in the strength, stiffness, and ductility characteristics of FRP-reinforced wood result even when $\rho_{fc} < \rho_{fc}^*$.

EXPERIMENTAL METHOD

CFRP-reinforced wood beams and beam columns were made and tested in three-point bending and eccentric axial loading, respectively. The fiber-composite material consisted of high-modulus carbon fibers at a volume fraction of 65%, bonded together with an epoxy matrix. The wood specimens were obtained from fir lumber with the strong material direction parallel to the member axis. Special efforts were made to obtain uniform and clean specimens without knots, to minimize the uncertainties associated with the variability in mechanical properties. The wood used in the beam-column eccentric loading tests came from a batch different from that used in the three-point bending tests.

The Young's modulus of wood was measured by recording the load-deflection behavior of four 760-mm-long beams with a cross section of 30 × 51 mm; the beams were loaded in three-point bending over a span of 686 mm. The yield strength and slope of the postyield branch of wood in uniaxial compression were measured by compressing four 25-mm cubes in an Instron testing machine. Finally, the tensile strength of wood was measured by loading four waisted wood specimens with cross sections of 4 × 7 mm in tension and recording the failure load.

A series of CFRP-reinforced beams were designed with varying area fractions of the composite reinforcement (series B). Each beam had a cross section of 30 × 51 mm and was 760 mm long. A list of the CFRP area fractions used for each of the different designs is given in Table 2. Three to five beams of each geometry were made by cutting the wood and CRFP
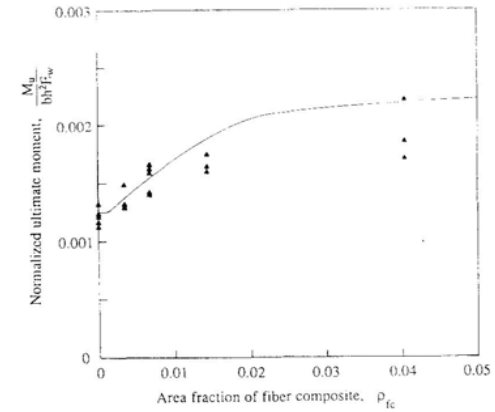
FIG. 14. Comparison between Analysis and Experimental Results for Normalized Ultimate Moment Capacity of CFRP-Reinforced Wood as Function of Fiber-Composite Area Fraction
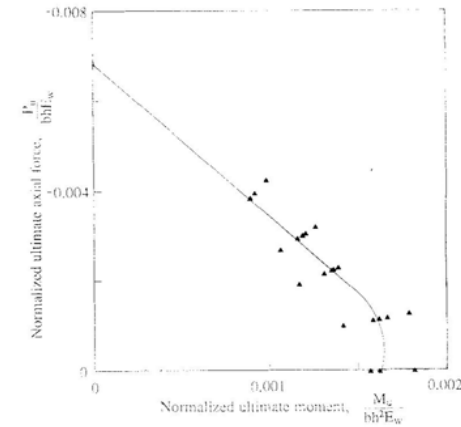
FIG. 15. Test Results Compared with Strength Model's Prediction for Eccentrically Loaded CFRP-Reinforced Wood Columns

to the correct size, then bonding them together with epoxy adhesive resin. The specimens were clamped together with weights while the adhesive cured for three days. The beams were loaded to failure in three-point bending over a span of 686 mm using roller supports and a screw jack to apply the load. Load and deflection at 45 mm from the point of load application were measured during the test with a load cell and a linear voltage differential transformer and were recorded on an X-Y recorder.

Another series of 51-mm long CFRP-reinforced beam colums were designed with a cross section of 25 × 19 mm and reinforcement area fraction

TABLE 5. Measured and Calculated Axial Loads and Bending Moments at Failure of FRP-Wood Eccentrically Loaded Columns (Series BC)

Average measured failure load (kN) (1)	Average measured moment (Nm) (2)	Calculated failure load (kN) (3)	Calculated failure moment (Nm) (4)
23.9	104.6	22.6	99.3
17.4	129.6	17.4	129.1
12.9	148.3	13.2	151.8
6.8	181.7	6.8	181.2
0.0	188.3	0.0	184.6

$\rho_{fc} = 0.0067$ (series BC). The members were loaded in eccentric compression at four different eccentricities e with respect to the centoid of the section and towards the face opposite to the composite reinforcement, as follows: $e = 1.65, 3.81, 9.52,$ and 23.8 mm. Three to five specimens were tested at each eccentricity, the ultimate load was recorded and from that, and the known eccentricity, the corresponding ultimate moment was calculated. Finally, corrections were made to the calculated ultimate moment to account for the effect of the P-delta phenomenon. The P-delta eccentricities were calculated by measuring the midspan deflection of the beam columns using a linear voltage differential transformer.

RESULTS

The data for Young's modulus, the slope of the postyield branch in uniaxial compression, and the stress and strain at compressive yield and tensile fracture obtained from uniaxial and three-point testing of the wood specimens are summarized in Table 3. It is evident that for the particular specimens used, the variability in material properties is remarkably low, even in uniaxial tension. The behavior is characteristic of defect-free materials, leading to the adoption of a high value for the stress distribution parameter $k (= 100)$, to imply that $f_m \approx f_t$. These results, along with the fiber-composite material properties listed in Table 1, were used to calibrate the analytical model for the bending/axial capacity of CFRP-reinforced wood.

Typical load-deflection curves from three-point bending tests on hybrid FRP wood beams are illustrated in Fig. 13. Initially, all are linear. Wood yield produced a nonlinear response terminated by a sudden drop of the load as a result of CFRP rupture. CFRP rupture was immediately followed by wood fracture in the tension zone, resulting in collapse of the specimens. Beams with high FRP area fractions yielded extensively, verifying the plastic hinge behavior.

Table 4 lists the calculated and average failure loads for each beam design tested; the results are also plotted in Fig. 14, illustrating a comparison between the measured and calculated normalized bending moment capacities. The overall agreement between the analysis and experiments is quite satisfactory for all the FRP area fractions used in this study. The combinations of theoretical and measured (average) axial loads and bending moments for each eccentric column tested are listed in Table 5; and a comparison between the theoretical and experimental bending moment-axial force interaction diagrams is illustrated in Fig. 15. A very good agreement between theory and the average experimental values is observed.

314

CONCLUSIONS

FRP-reinforced wood is a new type of hybrid construction material that has a strong potential for use in the design of lightweight yet low-cost structural elements. Reinforcing wood members with very thin fiber-composite sheets bonded on their tension face appears to be a promising way of increasing the strength, stiffness, and ductility characteristics of wood structures. The present study presents comprehensive strength models for the short-term behavior of hybrid FRP wood structures subject to bending or a combination of bending and axial loads.

The approximations inherent in the analysis stem from the need to describe the response of beams and beam columns by available uniaxial stress-strain relations for the constituent materials. The behavior of FRP-reinforced wood members is established from moment-curvature curves obtained by an incremental numerical procedure. Parametric studies were conducted to examine the effect of external reinforcement on the ultimate moment capacity, flexural rigidity, ductility, and axial force-bending moment interaction of FRP-reinforced wood. It is concluded that even very small area fractions of fiber-composite reinforcement result in significant improvements of the member's mechanical behavior. Upper limits to the amount of FRP to be used are established, beyond which the flexural capacity of the member levels off.

Test results obtained from three-point bending and eccentric compression tests confirmed the analysis for the failure loads and moments as well as the collapse mechanisms. It appears that when carbon FRP sheets are employed in the area fractions used for these experiments, failure is governed by wood compressive yield followed by rupture of the composite sheet which, in turn, produces tensile fracture of wood in the tension face.

Further work is needed to address long-term response issues, such as the durability, fatigue, and creep properties of the FRP wood hybrid system.

APPENDIX I. REFERENCES

"Basic panel properties of plywood overlaid with fiberglass-reinforced plastic." (1972). *Research Report No. 119, part 1*, Am. Plywood Assoc., Tacoma, Wash.

Bazan, I. M. M. (1980). "Ultimate bending strength of timber beams," PhD thesis, Nova Scotia Technical College, Halifax, Nova Scotia, Canada.

Biblis, E. J. (1965). "Analysis of wood-fiberglass composite beams within and beyond the elastic region." *Forest Prod. J.*, 15(2), 81–88.

Bodig, J., and Jayne, B. (1982). *Mechanics of wood and wood composites*. Van Nostrand Reinhold, New York, N.Y.

Bohannan, B. (1962). "Prestressed wood members." *Forest Prod. J.*, 12(12), 596–602.

Borgin, K. B., Loedolff, G. F., and Saunders, G. R. (1968). "Laminated wood beams reinforced with steel strips." *J. Struct. Engrg.*, ASCE, 94(7), 1681–1705.

315

Buchanan, A. H. (1986). "Combined bending and axial loading in lumber." *J. Struct. Engrg.*, ASCE, 112(12), 2592–2609.

Buchanan, A. H. (1990). "Bending strength of lumber." *J. Struct. Engrg.*, ASCE, 116(5), 1213–1229.

Bulleit, W. M., Sandberg, L. B., and Woods, G. J. (1989). "Steel-reinforced glued laminated timber." *J. Struct. Engrg.*, ASCE, 115(2), 433–444.

Coleman, G. E., and Hurst, H. T. (1974). "Timber structures reinforced with light gage steel." *Forest Prod. J.*, 24(7), 45–53.

Dziuba, T. (1985). "The ultimate strength of wooden beams with tension reinforcement." *Holzforschung und Holzverwertung*, 37(6), 115–119 (in German).

Hoyle, R. J. (1975). "Steel-reinforced wood beam design." *Forest Prod. J.*, 25(4), 17–23.

Hull, D. (1981). *An introduction to composite materials*. Cambridge Univ. Press, Cambridge, England.

Iyer, S. L., Sivaramakrishnan, C., and Atmaran, S. (1989). "Testing of reinforced concrete bridges for external reinforcement." *Proc. Sessions Related to Struct. Mater., Structures Congress '89*, ASCE, 116–122.

Kaiser, H. (1989). "Strengthening of reinforced concrete with epoxy-bonded carbon-fiber plastics," PhD thesis, ETH, Zurich, Switzerland (in German).

Kobetz, R. W., and Krueger, G. P. (1976). "Ultimate strength design of reinforced timber: Biaxial stress failure criteria." *Wood Sci.*, 8(4), 252–262.

Krueger, G. P. (1973). "Ultimate strength design of reinforced timber: State of the art." *Wood Sci.*, 6(2), 175–186.

Krueger, G. P., and Eddy, F. M. (1974). "Ultimate strength design of reinforced timber: Moment-rotation characteristics." *Wood Sci.*, 6(4), 330–344.

Krueger, G. P., and Sandberg, L. B. (1974). "Ultimate strength design of reinforced timber: Evaluation and design parameters." *Wood Sci.*, 6(4), 316–330.

Lantos, G. (1970). "The flexural behavior of steel reinforced laminated timber beams." *Wood Sci.*, 2(3), 136–143.

Meier, U. (1987). "Bridge repair with high performance composite materials." *Material and Technik*, 4, 125–128 (in German).

Mitzner, R. C. (1973). "Durability and maintenance of plywood overlaid with fiberglass reinforced plastic." *Res. Report No. 119, part 3*, Am. Plywood Assoc., Tacoma, Wash.

Peterson, J. (1965). "Wood beams prestressed with bonded tension elements." *J. Struct. Engrg.*, ASCE, 91(1), 103–119.

Ritchie, P. A., Thomas, D. A., Lu, L.-W., and Connelly, G. M. (1990). "External reinforcement of concrete beams using fiber-reinforced plastics." *Lehigh Univ. ATLSS Report No. 90-06*, Lehigh Univ., Bethlehem, Pa.

Saadatmanesh, H., and Ehsani, M. (1989). "Application of fiber-composites in civil engineering." *Proc. Sessions Related to Struct. Mater. Structures Congress '89*, ASCE, 526–535.

Saadatmanesh, H., and Ehsani, M. (1990). "Flexural strength of externally reinforced concrete beams." *Proc. Mater. Engrg. Congress '90*, ASCE, 1152–1161.

Sliker, A. (1962). "Reinforced wood laminated beams." *Forest Prod. J.*, 12(1), 91–96.

Stern, E. G., and Kumar, V. K. (1973). "Flitch beams." *Forest Prod. J.*, 23(5), 40–47.

Triantafillou, T. C., and Deskovic, N. (1991). "Innovative prestressing with FRP sheets: Mechanics of short-term behavior." *J. Engrg. Mech.*, ASCE, 117(7), 1652–1672.

Triantafillou, T., and Plevris, N. (1991). "Post-strengthening of r/c beams with epoxy-bonded fiber-composite materials." *Proc. ASCE Specialty Conf. on Advanced Composites for Civ. Engrg. Struct.*, ASCE, 245–256.

Weibull, W. (1939). "A statistical theory of the strength of materials." *Proc. No. 151*, Royal Swedish Inst. of Engineering Research, Stockholm, Sweden.

APPENDIX II. NOTATION

The following symbols are used in this paper:

b = width of cross section;
b_{fc} = width of fiber-composite sheet;
c = neutral axis depth as ratio of total beam depth;
E = Young's modulus;
E_{fc} = Young's modulus of fiber composite;
E_w = Young's modulus of wood;
e = eccentricity;
f_c = compressive strength of wood;
f_m = bending strength of wood;
f_t = tensile strength of wood;
h = depth of beam cross section;
I = moment of inertia;
k = stress distribution effect parameter;
l = beam length;
M = bending moment;
M_u = ultimate bending moment;
m = ratio of slopes in compressive stress-strain relationship for wood;
P = axial force;
P_u = ultimate axial force;
t = thickness of fiber composite;
ε_b = strain at bottom fiber;
ε_c = strain corresponding to the compressive strength of wood;
ε_t = strain corresponding to the tensile strength of wood;
ε_{fc}^* = uniaxial strain of fiber composite at failure;
ρ_{fc} = area fraction of fiber composite;
ρ_{fc}^* = critical area fraction of fiber composite;
ϕ = curvature;
ϕ_m = maximum curvature; and
ϕ_y = curvature at first yield.